Dislocations and Etch Figures in High Purity Zinc*

R. C. BRANDT, K. H. ADAMS, AND T. VREELAND, JR.
W. M. Keck Laboratory of Engineering Materials, California Institute of Technology, Pasadena, California
(Received 29 August 1962)

A method of etching high purity zinc single crystals to reveal various etch figures on {10$\bar{1}$0} planes is presented in the preceding paper. The procedure involves the introduction of mercury to the crystal surface prior to a chemical polish with dichromic acid. The mercury was found to be concentrated at the etch figures. This paper presents the results of several experiments which support the conclusion that there exists a one-to-one correspondence between etch figures and dislocations. Some observations of slip on (0001) basal planes and {1$\bar{2}$12} pyramidal planes, and of twinning in zinc are also presented.

INTRODUCTION

SEVERAL questions should be asked about the application of an etching procedure to reveal dislocations. First, do all the etch patterns produced correspond to dislocations; and second, are all of the dislocations revealed? In answer to the first question, several qualitative observations of etch patterns were made to see if all of the etch figures observed could be attributed to dislocations. In answer to the second question, several quantitative tests were made to check theoretical predictions of the dislocation density and configuration. The etch figures examined were produced on {10$\bar{1}$0} prism surfaces.

QUALITATIVE OBSERVATIONS

Several specimens were observed after etching and again after repolishing and re-etching to determine the reproducibility of the etch markings with depth in the crystal. The repolishing removed from 100 to 200 μ of the surface. The reproducibility of etch figures with depth follows the pattern expected if each figure is associated with a dislocation.

Complex pip patterns are observed on a crystal surface in the regions where local deformation has occurred. Such a pattern is shown in Fig. 1 where the local deformation was produced by scratching the surface with a diamond stylus.

Etch figures are redistributed when deformed crystals are annealed. Subboundaries are revealed by the etchant, and the density of figures between subboundaries is reduced by annealing.

QUANTITATIVE TESTS

The density of etch figures produced by bending the [$\bar{1}$2$\bar{1}$0] axis of crystals about their [10$\bar{1}$0] axis was determined. Three 99.999% purity crystals were bent to a radius of 7.5 cm. The Nye formula predicts that a dislocation density, $\rho=(rb)^{-1}$, produces a radius of curvature r, where b is the magnitude of the Burgers vector and the dislocations are all of the same sign and of the same slip system. If it is assumed that only basal dislocations of one sign are produced by the bending experiments, the density of dislocations corresponding to a radius of 7.5 cm in zinc is 51×10^5 cm^{-2}, taking $b=2.66$ Å (lattice parameter in the [1$\bar{2}$10] direction). The average density of figures observed in the test crystals in excess of the initial density was $54\pm10\times10^5$ cm^{-2}. These crystals were etched within several minutes after bending, and the density of figures agrees with the Nye formula within the limits of experimental error. This indicates that only a relatively small fraction of the dislocations formed in the bending differ in sign, or

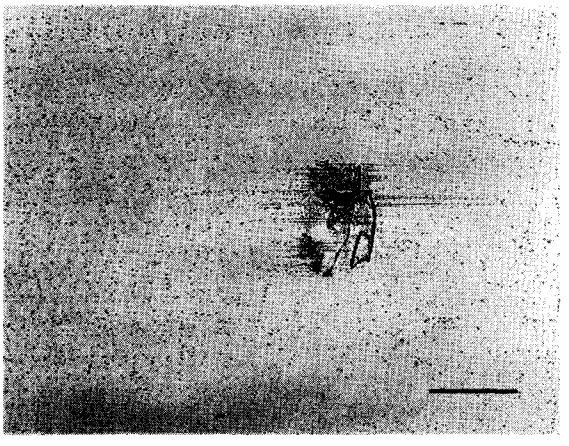

FIG. 1. Etch figures resulting from surface deformation. Magnification ×100.

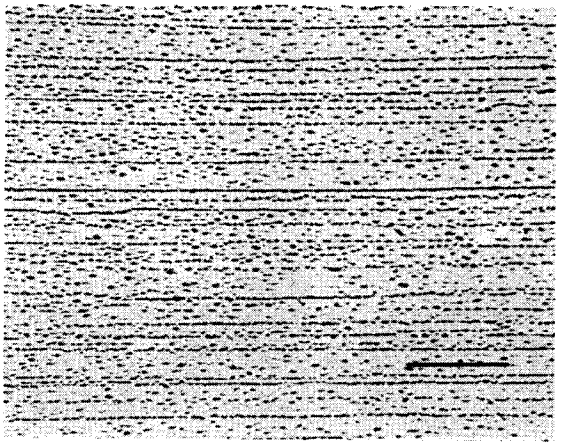

FIG. 2. Etch figures resulting from torsional deformation about a [0001] axis. Magnification ×500.

* This work was supported by the U. S. Office of Naval Research.

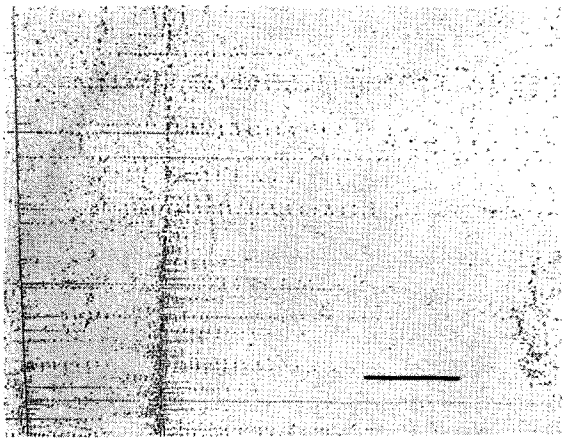

FIG. 3. Dislocations piled-up on subboundaries. Magnification ×100.

that most of the dislocations which differ in sign were annihilated before the crystals were etched.

Linear arrays of etch figures are observed that lie perpendicular to the basal planes. If these figures correspond to individual edge dislocations, the array is a tilt boundary of angle $\theta=b/h$, where h is the spacing of the figures. The angle of a tilt boundary in a zone refined crystal was measured by means of an interference microscope on a cleaved (0001) basal plane. The interference measurement gave $\theta=1.9\pm0.2\times10^{-4}$ rad. The separation of figures was measured on a $(10\bar{1}0)$ plane adjacent to the cleaved surface. The angle calculated from the figure spacing gave $\theta=1.82\pm0.04\times10^{-4}$ rad. These values agree within the limits of experimental error. The figures must therefore correspond to individual edge dislocations.

Hexagonal networks of screw dislocations that lie on basal planes in zinc have been observed by Berghezan *et al.* by transmission electron microscopy.[1] These networks result from twist about a [0001] axis of the crystal.[2] If the networks are composed of screw dislocations of length s and the networks are equally spaced with a density of z per unit length along the [0001] axis, the twist per unit length is $\phi=zb/\sqrt{3}s$. The density of screw dislocations intersecting the $(10\bar{1}0)$ plane is then $2\phi/\sqrt{3}b$. A crystal of 99.999% purity was twisted about its [0001] axis and the twist was measured to be 0.42 ± 0.02 rad/cm. The figures on a $(10\bar{1}0)$ surface of this crystal are shown in Fig. 2, and their density was determined to be $19\pm3\times10^{6}\text{cm}^{-2}$. The density calculated from the above formula with the measured values of twist and b for a complete basal dislocation is $18.2\pm0.9\times10^{6}\ \text{cm}^{-2}$. The difference between the observed and calculated densities should represent the initial dislocation density. The initial density was not determined, but similar crystals have background densities that range from 0.4×10^{5} to $20\times10^{5}\ \text{cm}^{-2}$. The density of figures in the twisted crystal therefore corresponds, within the limits of experimental error, to the density of screw dislocations predicted by the model.

While the experimental evidence presented above does not prove that all dislocations intersecting $\{10\bar{1}0\}$ surfaces are revealed by the etching procedure, it indicates strongly that all edge and screw dislocations that lie on (0001) planes are revealed, and that each etch figure represents the intersection of a dislocation with the surface. Qualitative observations presented in a subsequent section indicate that nonbasal dislocations are also revealed on prism surfaces.

SUBBOUNDARIES

Examination of a number of crystals after small amounts of deformation reveals that the dislocation distribution around subboundaries is very different from the distribution between subboundaries. The number of dislocations piled up on the boundaries shown in Fig. 3 indicates that the boundaries are relatively effective

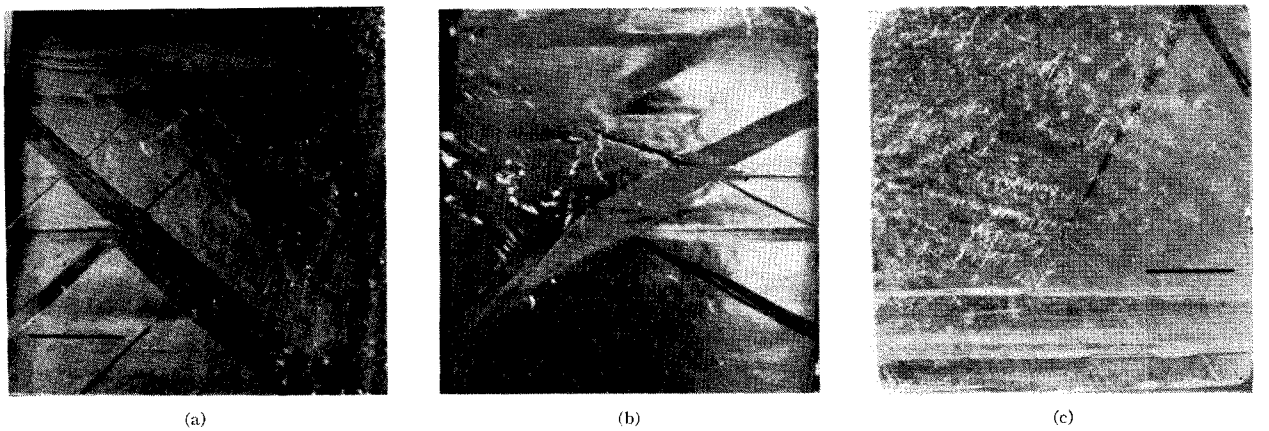

(a) (b) (c)

FIG. 4. Unetched compression specimen. Plane of untwinned material: (a) $(10\bar{1}0)$, (b) $(\bar{1}2\bar{1}0)$, and (c) (0001). Magnification ×6.

[1] A. Berghezan, A. Fourdeux, and S. Amelinck, Acta Met. **9**, 464 (1961).
[2] N. Brown, Trans. Am. Inst. Mining, Met., Petrol. Engrs. **203**, 134 (1955).

(a)

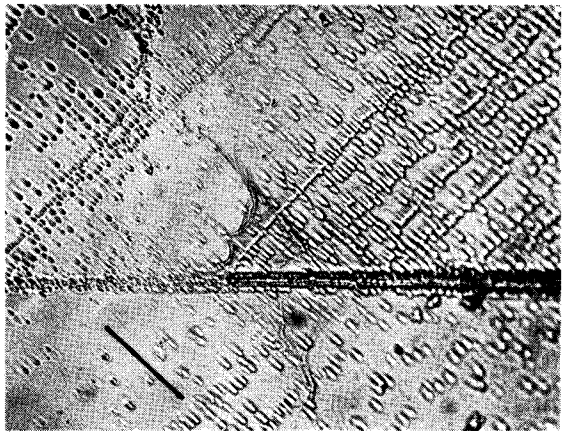

(b)

FIG. 5. Etch figures associated with twin tips. (a) Compression specimen. Magnification ×750. (b) Accidental damage. Magnification ×500.

obstacles to dislocation motion. These boundaries may be simple tilt boundaries, or more complex subboundaries. Li[3] concludes from theoretical calculations that a simple tilt boundary is not a very effective barrier to the penetration of parallel dislocations of the same Burgers vector. If, however, the probability is high that a moving dislocation will meet a boundary before some other obstacle is encountered, the boundaries will act as the more effective obstacles. This is the case in zinc crystals of high purity with low dislocation density between subboundaries.

NONBASAL SLIP AND TWINNING

The correspondence between etch figures and nonbasal dislocations was investigated in a crystal deformed by a loading procedure that minimized basal slip. A zone refined crystal was loaded in compression along the [0001] axis until twinning occurred. Deviation from a linear load-deflection curve was noted at a compressive stress of 1450 psi. This could result from pyramidal slip on $\{1\bar{2}12\}$ planes in the $\langle 1\bar{2}1\bar{3}\rangle$ direction at a resolved shear stress of 600 psi. Such nonbasal deformation has been reported by Bell and Cahn.[4] Twinning occurred at a shear stress of 3000 psi, resolved in the $\{1\bar{1}02\}$ twinning plane. Figure 4 illustrates twin traces on $(10\bar{1}0)$, (0001), and $(\bar{1}2\bar{1}0)$ planes of the unetched specimen.

The $(10\bar{1}0)$ prism plane of the compression specimen was etched to observe the pip arrays associated with twins. Etching of twinned material produced a rough finish due to the fact that the surface was misoriented from a $\{10\bar{1}0\}$ plane. Figure 5 illustrates the appearance of twinned and untwinned material and several pip arrays associated with the tips of twins. Figure 5(a) is a $(10\bar{1}0)$ surface of the compression specimen and Fig. 5(b) is a $(10\bar{1}0)$ surface of a specimen of similar initial dislocation density which was accidentally damaged. The large increase in background density in the compressed specimen is the result of nonbasal slip before twinning. Pips lined up parallel to the twin tips and tilt boundaries eminating from tips represent accommodation deformation as explained by Rosenbaum.[5] The slip lines corresponding to (0001) basal slip as seen in Fig. 4 result from similar accommodation to the high stress regions at twin intersections.

To study the deformation within twinned material, a $(10\bar{1}0)$ prism face was exposed by sectioning the compression specimen with an acid saw almost parallel to the (0001) basal plane of the untwinned material. The surfaces of the twinned material, as seen in Fig. 4(c), are within 0.1° of the $\{10\bar{1}0\}$ prism planes. The specimen was sectioned in order to examine regions that were not affected by slight inhomogeneities in the load applied to the ends. Figure 6 shows pip patterns revealed on a $(10\bar{1}0)$ face of twinned material. Pips labeled P can be observed running parallel to the $(1\bar{2}12)$ slip plane

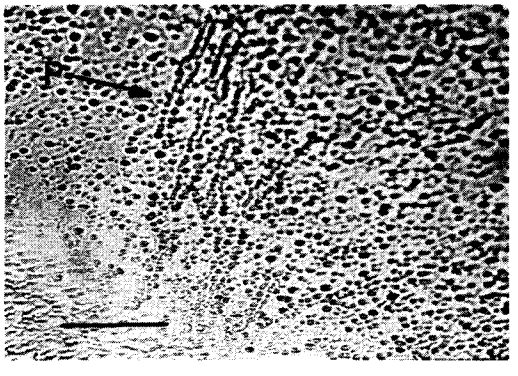

FIG. 6. Etch figures in twinned material of compression specimen. Magnification ×500.

[3] J. C. M. Li, Acta Met. **8**, 296 (1960).

[4] R. L. Bell and R. W. Cahn, Proc. Roy. Soc. (London) **A239**, 494 (1957).

[5] H. S. Rosenbaum, Acta Met. **9**, 742 (1961).

trace which may indicate that the pips correspond to pyramidal slip dislocations. The pip arrays in Figs. 5 and 6 only occur in short segments and are not restricted to narrow bands. This results from the fact that there are six intersecting $\{1\bar{2}12\}$ planes each with the same resolved shear stress. Interaction of the dislocations on different intersecting slip planes prevents the formation of slip bands such as those observed on the basal planes. This also explains the absence of $\{1\bar{2}12\}$ pyramidal slip lines on the specimen surface in Fig. 4.

SUMMARY AND CONCLUSIONS

The qualitative and quantitative observations of etch figures given above support the conclusion that all basal dislocations which intersect the prism surfaces are revealed by the etching procedure. The qualitative observations of etch figures on specimens that have been deformed by nonbasal slip and twinning support the conclusion that there is a one to one correspondence between dislocations and etch figures on prism surfaces of high purity zinc.

JOURNAL OF APPLIED PHYSICS VOLUME 34, NUMBER 3 MARCH 1963

Theory of Nernst Generators and Refrigerators

M. H. NORWOOD
Corporate Research & Engineering, Texas Instruments Incorporated, Dallas 22, Texas
(Received 23 April 1962)

Formulas for efficiency and coefficient of performance are derived for devices based on the Nernst and Ettingshausen effects. The equations reduce to those of Harman and Honig in the limits of small figure of merit and refrigerator current, but they do not approach the Carnot limits. To obtain a better device theory, one must solve a two-dimensional partial differential equation in which the current density is allowed to vary with position.

A crude maximization procedure for the figure of merit is shown for a one-band nondegenerate semiconductor in a weak magnetic field. Experimental data indicate that Hg_xCd_{1-x} Te alloys are perhaps the best materials for such devices at present.

INTRODUCTION

IN 1958, O'Brien and Wallace[1] derived an expression for the maximum ΔT of a thermomagnetic refrigerator in terms of the Ettingshausen coefficient P. Their formulas resembled those for thermoelectric devices. More recently, Harman and Honig,[2] Angrist,[3] and El-Saden[4] have derived expressions for device behavior of generators in addition to an expression for the coefficient of performance of a refrigerator. These expressions indicate there are significant differences between thermoelectric and thermomagnetic devices. The work reported in this paper agrees with that of Harman and Honig and that of Angrist but it appears that all answers derived thus far are approximate.

It should be emphasized that this designation of a "thermomagnetic" device is not related to the devices proposed by Elliot,[5] by Brillouin and Iskenderian,[6] and by others which depend on a rapid change in magnetic permeability near the Curie point.

The fundamental field and heat current density equations which govern the behavior of thermoelectric (TE) and thermomagnetic (TM) devices have been formulated by Callen[7] using principles of irreversible thermodynamics.[8,9]

$$-\nabla V=\rho\mathbf{j}+\alpha(\nabla T)+R(\mathbf{B}\times\mathbf{j})-Q(\mathbf{B}\times\nabla T), \quad (1)$$

$$\mathbf{q}=\alpha T\mathbf{j}-\kappa(\nabla T)-QT(\mathbf{B}\times\mathbf{j})+\kappa S(\mathbf{B}\times\nabla T). \quad (2)$$

Equations (1) and (2) are simply Callen's equations written in vector form with certain differences in signs and symbols. If the magnetic field $\mathbf{B}$ is in the z direction and all currents, heat flows, and temperature gradients lie in the xy plane, then only the x and y components in Eqs. (1) and (2) must be considered. In these equations, R, Q, and S are the isothermal Hall, Nernst, and Righi-Leduc coefficients, respectively. These equations follow the sign conventions adopted by Wilson[10] and differ from Callen's. The coefficients R and S will be positive for p-type and negative for n-type material. The coefficient Q will depend, however, not on the type carrier, but on the scattering mechanisms involved. If the scattering relaxation time depends on the energy according to the simple relation $\tau(E)=AE^s$,

[1] B. J. O'Brien and C. S. Wallace, J. Appl. Phys. **29**, 1010 (1958).
[2] T. C. Harman and J. M. Honig, Bull. Am. Phys. Soc. **7**, 332 (1962); **7**, 410 (1962).
[3] S. W. Angrist, Paper to be presented to ASME Meeting, Heat Transfer Division, Houston, Texas, August 1962.
[4] M. R. El-Saden, J. Appl. Phys. **33**, 1800 (1962).
[5] J. F. Elliot, J. Appl. Phys. **30**, 1774 (1959).
[6] L. Brillouin and H. P. Iskenderian, Elec. Commun. **25**, 300 (1948).
[7] H. B. Callen, Phys. Rev. **85**, 16 (1952).
[8] S. R. DeGroot, *Thermodynamics of Irreversible Processes* (Interscience Publishers, Inc., New York, 1952).
[9] C. A. Domenicali, Revs. Mod. Phys. **26**, 237 (1954).
[10] H. A. Wilson, *Theory of Metals* (Cambridge University Press, New York, 1953).